Materials Chemistry and Physics 344 (2025) 131097

Contents lists available at ScienceDirect

Materials Chemistry and Physics

journal homepage: www.elsevier.com/locate/matchemphys

Isoniazid adsorption and release by Cloisite and Laponite: An effect of surface charge

Jessica de Carvalho Arjona [a,b], Mazen Samara [a], Carina Ulsen [c], Francisco Rolando Valenzuela Diaz [b], Nicole Raymonde Demarquette [a,*]

[a] Mechanical Engineering Department, École de Technologie Supérieure, Montréal, QC, H3C 1K3, Canada
[b] Departamento de Engenharia Metalúrgica e de Materiais, Escola Politécnica, Universidade de São Paulo, São Paulo, 05508-030, Brazil
[c] Departamento de Engenharia de Minas e de Petróleo, Escola Politécnica, Universidade de São Paulo, São Paulo, 05508-030, Brazil

HIGHLIGHTS

- Smectite surface charges are crucial for isoniazid adsorption in acidic media, particularly due to the drug's protonation.
- An acidic environment enhances the montmorillonite adsorption capacity of INH, increasing it from 12 mg/g to 115 mg/g.
- The acid form of isoniazid significantly influences its adsorption by Cloisite and Laponite.
- The release behavior of INH from the clay varies depending on the pH of the surrounding media.
- Cloisite demonstrated higher drug incorporation and a more controlled release rate compared to Laponite.

GRAPHICAL ABSTRACT

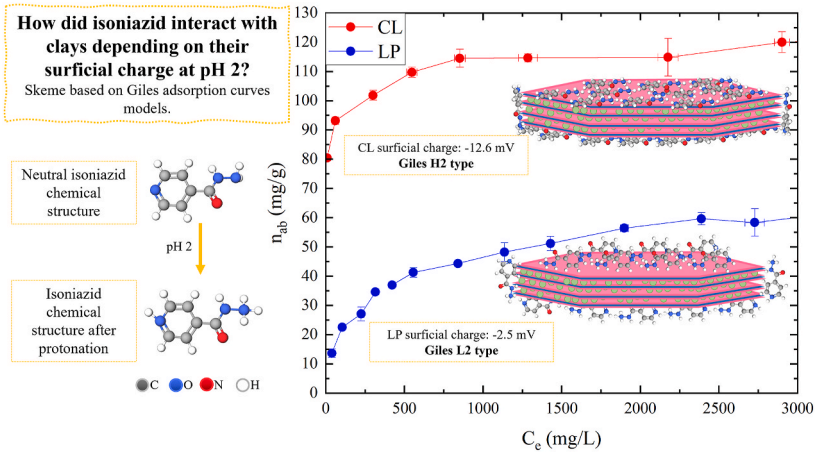

ARTICLE INFO

Keywords:
Isoniazid
Montmorillonite
Laponite
Drug delivery systems
Controlled release

ABSTRACT

Two different smectites, Cloisite (CL), a montmorillonite, and Laponite (LP), a synthetic hectorite-like clay, were investigated for their efficiency in isoniazid (INH) adsorption and release mechanisms. Adsorption was conducted at an acidic pH = 2 to leverage the protonation effect of INH. At acidic pH, the clays exhibited different surface charges: −12 mV for CL and −2 mV for LP, indicating a stronger negative charge on CL. These changes affected the INH incorporation and release, increasing the attachment on the clay surface. CL, the clay with the lowest surface charge, manifested a higher incorporation of INH, 115 mg/g, and a more controlled release of INH in the stomach environment (less than 8 %, against 25 % for LP). These values compared favorably with those cited in the literature and demonstrated a potential for drug delivery. Although X-ray diffraction (XRD) did not show an increase in the basal distance for either clay, Fourier-transform infrared spectroscopy (FTIR) and thermogravimetry analysis (TGA) showed the interaction between clay and drug after the incorporation. Compared to literature, the hybrids developed in this study exhibited higher drug loading and a more effective

* Corresponding author.
E-mail address: nicoler.demarquette@etsmtl.ca (N.R. Demarquette).

https://doi.org/10.1016/j.matchemphys.2025.131097
Received 3 February 2025; Received in revised form 16 May 2025; Accepted 26 May 2025
Available online 27 May 2025

pH-responsive release, particularly at pH 2. This is especially important for oral drug delivery, where protecting the drug in the stomach and enabling its release in the intestine can enhance bioavailability. These findings underscore the potential of smectite clays as promising candidates for INH-controlled release and contribute to identifying key-clay characteristics for effective oral drug delivery systems.

1. Introduction

Isoniazid (INH) is a drug used globally in tuberculosis treatment. It is often administered alongside other medications, which can interact and reduce bioavailability, necessitating high doses of up to 300 mg/day [1]. These high doses can lead to various side effects, decreasing patient compliance, and increasing the proliferation of resistant bacteria. To improve drug bioavailability, drug delivery (DD) systems are often employed [2]. In this study, DD systems were considered as modified-release systems typically used to achieve a gradual drug release, thereby avoiding higher drug concentrations in the bloodstream and potentially decreasing the treatment side effects.

In most cases, the drug is incorporated into a vehicle, which may also protect it from environmental reactions. INH is an ideal candidate for such systems because its chemical structure contains a pyridine ring and a hydrazine group, both of which can influence its interaction with other materials [3,4]. These groups can protonate in an acidic environment, altering the drug state and how it interacts with the surroundings [5]. Various drug DD systems have been explored for INH, including polymeric particles [6–10], 3D printed polymeric pills [11], inorganic particles such as zeolites [5,12], silica particles [4], layered double hydroxides (LDHs) [13], clays from different groups, such as palygorskite [3,14,15], montmorillonite [16–19], halloysite [2,20], or a combination of polymeric and inorganic particles [21–24].

Clay and other inorganic particles, like layered double hydroxides (LDH) [25,26], are commonly used for drug delivery systems. Their efficiency as DD systems is essentially related to their ability to incorporate spontaneously [12,14,17,20] and release drugs like INH, which occurs through interactions between the clay surface and the drug [15,16]. Recent studies also investigated the influence of clay surface modification in mesoporous silicate to verify the influence of surface polarity of acidic drug molecules, as INH, under acidic pH, which can provide a useful perspective on surface-drug interactions [26]. Other studies also employed computational modeling to examine drugs intercalation and release mechanisms by LDHs [25] and zeolite [5], offering valuable theoretical insights. While these studies differ in terms of materials and approach, our work complements them by providing empirical evidence based on smectite clays, which helps validate and contextualize computational predictions and expands the understanding of pH-dependent release mechanisms using naturally occurring clay minerals.

In this work, Cloisite (CL), a commercial natural clay [28], and Laponite (LP), a synthetic clay [27], were used to study the influence of their surface charge on INH incorporation. Their surface charge is directly dependent on their chemical composition. They belong to the phyllosilicate group, characterized by a t-layered structure (Fig. 1-a). Their layers are formed following a TOT (Tetrahedral-Octahedral-Tetrahedral) format: two tetrahedral sheets of silicon oxide are separated by an octahedral metal oxide sheet. For hectorite-like clays (HCT), such as LP, the metal is magnesium (Mg^{+2}), the clay is called trioctahedral and all octahedral spaces are occupied (Fig. 1-b,d,e). For montmorillonite (MMT), such as Cloisite (CL), the metal is aluminum (Al^{+3}), the clay is called dioctahedral, and only two-thirds of the octahedral spaces are occupied (Fig. 1-c,f,g). During clay formation, ions dissolved from the original rocks may replace specific atoms in the clay minerals' crystal structure through isomorphic substitution, leading a permanent negative surface charge. [29,30]. These substitutions generate a surface charge that must be neutralized by exchangeable cations situated between the layers. These cations can vary in type, depending on the mineral availability in the previous rock during the crystallization process. In the present work, sodium (Na^{+}) is the primary cation used. In addition to the negative surface charge inherent in clays, they contain hydroxyl groups at the edge of their crystals, which influence their behavior in acidic environments. In acidic conditions, H^{+} ions can replace the clay's exchangeable cations, penetrate the crystal structure, and react with the hydroxyl group, increasing the clay's surface charge. This surface charge change can positively impact the adsorption and the desorption/release of certain drugs [4].

Due to their chemical structure, clays can interact with many drugs through hydrogen bonding, van der Waals forces, and cation exchange [27]. Furthermore, the environmental pH can affect the chemical structures of both the clay and the drug, changing their interactions. In the case of INH, its pH-dependent behavior could enhance the adsorption in acidic conditions due to the increase of acid-base interactions between the silanols groups on the clay and the INH pyridine and hydrazide groups, which boosts the clay's adsorption capacity [3,4]. Furthermore, clay/INH composite has the potential to be effective for drug delivery, with the clay providing protection at pH 2 and ensuring

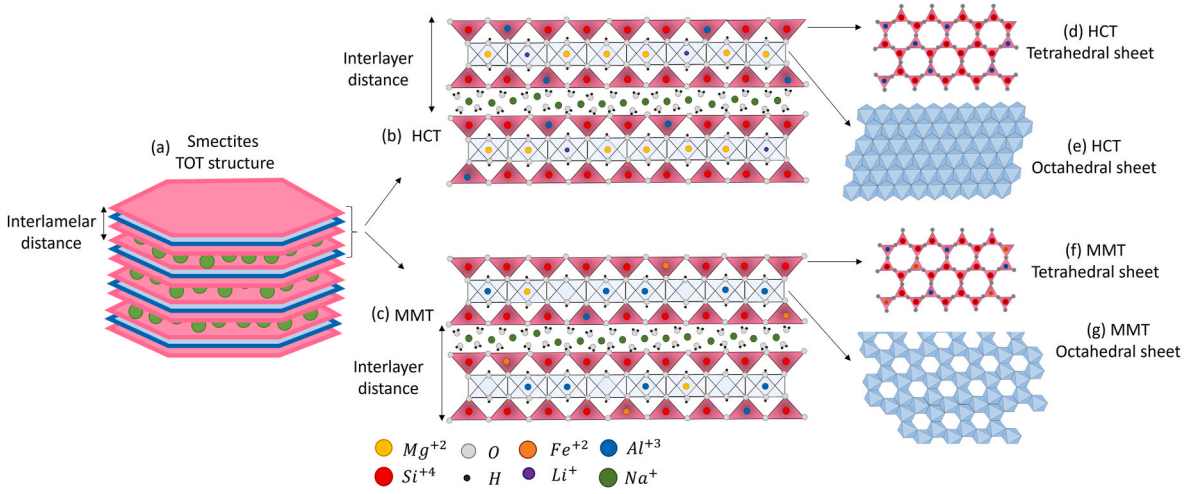

Fig. 1. Smectite structures and the crystal difference between montmorillonite (MMT) and hectorite-type clay (HCT).

effective release at pH levels higher than 6.8. The adsorption mechanism and thermodynamics of neutral INH incorporation by montmorillonite were described before [17]. However, few studies have reported a controlled release of INH from this clay type. Most studies observed a complete release within 10 min [2,5,13], additionally, the ones that presented a pH-dependent release reported a release of a small amount of the drug, around 4–11 mg/g [3,4].

In turn, the ability of clays to incorporate drugs can be evaluated by measuring the adsorption efficiency of a solute onto a solid adsorbent, which can be assessed using Giles' methodology [5,14,17,20,31–33]. This method links the shape of the adsorption curves to the underlying physical mechanism of adsorption. Since the interaction and orientation of the solute on the adsorbent surface influence the shape of the adsorption curves [34,35], it is possible to infer the conformation of solute molecules within the adsorbent. Giles' methodology provides valuable information on the conformation of solute molecules in adsorbents.

It is known that the pH affects the clay-INH incorporation. The main objective of this study was to investigate how clays with similar structures, but different surface charges, interact with the drug. The adsorption studies were conducted in two environmental pH levels (2 and 7). Gile's methodology was used to analyze the clay/drug interactions. The *in vitro* release test evaluated the hybrids' behavior in the oral release and two different pH levels, 2.0 and 7.4, for 5 h. To our knowledge, the study of adsorption and release of isoniazid influenced by pH has not been conducted using smectite group clays. The main objective of this work was to investigate how differences in the chemical composition of montmorillonite and hectorite clays can impact their ability to incorporate and release INH. Smectite clays were selected due to their natural abundance, low cost, biocompatibility, and established use in pharmaceutical and cosmetic applications. Their high surface area, swelling ability, and ease of modification make them promising candidates for drug delivery systems, and this study aims to better understand the key properties that govern their performance. To further elucidate the influence of pH on controlled release, the clays were characterized in terms of their clay/INH interaction. Thermogravimetric analysis (TGA) was used to verify the presence of INH after adsorption; Fourier transformation Infrared spectroscopy (FTIR) was employed to examine the interaction between the drug and the clay; and X-ray diffraction (XRD) was utilized to determine whether the drug intercalated the clay lamellas.

2. Materials and methods

2.1. Materials

Isoniazid, $NaHPO_4$, NaCl, NaOH, and 37 % HCl solution were analytical-grade reagents purchased from Sigma-Aldrich. The clays used in this study, Laponite (LP) and Cloisite Na^+ (CL), were kindly provided by BYK Additives and Instruments (Germany). All materials were used without further purification. The chemical composition and loss on ignition (LOI) of the clays are presented in Table 1. These values were determined by X-ray fluorescence (XRF) using a Zetium Malvern Panalytical instrument; additional characterization details are available in Ref. [18]. Due to the low atomic number of lithium, its concentration could not be determined by XRF and was instead quantified by strong mineral acid block digestion followed by inductively coupled plasma triple quadrupole mass spectrometry (ICP-QQQ), following a modified EPA 200.8 method. The lithium content was found to be 71.1 ppm in CL and 3326 ppm in LP, consistent with expectations.

The clays' cation exchange capacity (CEC) was determined using representative samples previously dried in an air oven at 105 °C for 24 h. The effective CEC was measured using the ammonium acetate method, followed by analysis via inductively coupled plasma optical emission spectrometry (ICP-OES). The resulting CEC values and the concentrations of exchanged cations are summarized in Table 2.

2.2. Methods

2.2.1. Zeta potential

Zeta potential measurements were made using a Malvern Zetasizer Nano. Before measurements, 0.1 % (w/v) aqueous dispersions were prepared at pH 2 and 7 and sonicated for 10 min. For each clay, the surface charge was measured in three different aliquots, with each aliquot tested three times.

2.2.2. Adsorption isotherms

Adsorption isotherms were performed using both clays at pH 2 and pH 7. A dry weight of 0.1 g of each clay was placed inside a dialysis tubing cellulose membrane, which retains molecules with molecular weight up to 14,000 Da, and immersed in 10 mL of INH solution, varying the concentration from 68.5 to 3082.5 mg/L (0.5–22.5 mmol/L). The system was stirred magnetically for 3 h [18], after which, the remaining concentration of INH in the solution was determined by a Thermo Scientific Evolution 260 Bio UV–visible spectrophotometer (UV–vis), with different calibration curves for each pH studied.

The amount INH incorporated per gram of clay (n_{ab}) was calculated as the difference between the initial quantity of INH (Q_i) and the remaining quantity (Q_e) in the supernatant after each time interval (Eq. (1)). Here n_{ab} represents the quantity of isoniazid adsorbed per gram of clay; Q_i is the initial amount of INH in the solution at the start of the experiment (also measured by UV–vis), Q_e is the amount of INH remaining in the supernatant at the end of the experiment, measured by UV–vis using the calibration curve, and m is the mass of the clay.

$$n_{ab} = \frac{Q_i - Q_e}{m} \quad \text{Eq. 1}$$

At the end of the experiment, a curve of q_{ab} (the amount in moles of INH adsorbed) as a function of Ce (the concentration at equilibrium after adsorption) was plotted and the data fitted to two different mathematical models: Langmuir (Eq. (2)) and Freundlich (Eq. (3)) using a nonlinear regression methodology, minimizing the sum of squared residuals (SSR) for each model. SSR is defined as the sum of the squared differences between the experimental adsorption data and the model-calculated adsorption as shown in Eq. (4). For the Langmuir model, the RL factor (Eq. (5)) was also calculated to verify the adsorption

Table 2
Cation Exchange Capacity and the percentage of ions released in CEC base saturation for CL and LP.

	CL	LP
CEC (mEq/100 g)	113.21	87.18
Percentage of Ions Released in CEC Base Saturation		
Na^+ (%)	75.20	90.20
Mg^{2+} (%)	2.77	4.77
K^+ (%)	1.04	0.27
Ca^{2+} (%)	21.00	4.76

Table 1
Chemical composition of Cloisite and Laponite.

Analyte	SiO_2	Al_2O_3	Fe_2O_3	MnO	MgO	CaO	Na_2O	K_2O	TiO_2	P_2O_5	LOI
CL (%)	59.50	21.30	4.24	<0.10	2.37	0.47	3.84	<0.10	0.12	<0.10	7.03
LP (%)	58.30	0.11	<0.10	<0.10	27.20	0.14	2.93	<0.10	<0.10	<0.10	11.00

strength at the two pH levels.

$$n_{ab} = \frac{K_L Q_m C_e}{1 + K_L C_e} \quad \text{Eq. 2}$$

$$n_{ab} = K_F C_e^{\frac{1}{n_F}} \quad \text{Eq. 3}$$

$$SSR = \sum_{i=1}^{m} \left(q_{i,exp} - q_{i,model}\right)^2 \quad \text{Eq. 4}$$

$$R_L = \frac{1}{1 + Q_m K_L} \quad \text{Eq. 5}$$

where n_{ab} is the amount of drug adsorbed, K_L is the Langmuir constant, Q_m is the theoretical amount of drug adsorbed at equilibrium, C_e is the equilibrium concentration, K_F is the Freundlich constant, and n_F is the Freundlich constant.

2.2.3. Kinetic drug release

The kinetic drug release test was performed for CL/INH and LP/INH hybrids prepared at pH 2, as they exhibited higher adsorption capacities than the ones prepared at pH 7. The release test simulated oral drug administration, where 100 mg of the clay/INH hybrid was inserted inside a dialysis tubing cellulose membrane with a molecular weight cutoff of 14,000 Da. The membrane bag was immersed in a pH 2 buffer solution for 2 h to simulate the stomach environment. It was then transferred to a pH 6.8 buffer solution for another 2 h, simulating the environment of the first zone of the intestine, and finally kept in a pH 7.4 buffer solution for an additional 4 h, simulating the second zone of the intestine. The buffer solutions were made according to a previous study [4]: i. pH 2: 1 g of NaCl and 0.5 mL of HCl in 1000 mL of water; ii. pH 6.8: 0.4 g of NaOH, 2.0 g of $NaH_2PO_4{\cdot}H_2O$, and 3.1 g of NaCl dissolved in 1000 mL; iii. pH 7.4: 2.5 mol/L NaOH was used to adjust the pH 6.8 solution. The release was monitored for 8 h (480 min). Samples were withdrawn and analyzed after the initial 10 min, and then every 30 min. After each sample was collected, the total volume of the solution was kept constant by adding the appropriate amount of buffer solution.

Since the pH affects the absorbance and wavelength of INH, three separate calibration curves were generated for 265 nm (pH 2) and 261 nm (pH 6.8 and 7.4) wavelengths. All the experiments were conducted in triplicate. The release data obtained were fitted to three different release models: Zero order (Eq. (6)), Korsmeyer-Peppas (Eq. (7)), and Higuchi (Eq. (8)).

$$\frac{M_t}{M_\infty} = K_0 t \quad \text{Eq. 6}$$

$$\frac{M_t}{M_\infty} = K t^n \quad \text{Eq. 7}$$

$$\frac{M_t}{M_\infty} = K_h t^{0.5} \quad \text{Eq. 8}$$

Where M_t is the amount of INH released after each interval (t), M_∞ is the amount of INH at the beginning of the experiment, K and n are Korsmeyer-Peppas constants, and K_h is the Higuchi constant.

2.2.4. Characterization

The same hybrids used for the release test were characterized using the following techniques: TGA, FTIR, and XRD. For TGA, a Pyris Diamond TG/DTA by Perkin Elmer was used to assess the mass loss of the pristine clay and its corresponding hybrid. The experiments were conducted under an airflow of 100 mL/min, a temperature range of 40–800 °C for clays and clay/INH hybrids, and 40–600 °C for pure INH. The temperature was increased at a rate of 10 °C/min. FTIR spectra were obtained using a PerkinElmer Spectrum Two FT-IR spectrometer, with analyses performed in the wavenumber range of 4000 cm^{-1} to 600 cm^{-1} at a resolution of 4 cm^{-1}. To conduct the FTIR test, a certain amount of each sample was deposited on the a priori cleaned crystal. A pressure of 70 Gauge was applied to it to minimize the signal noise. XRD spectra were recorded using a Malvern Panalytical Empyrean DY-2516 X-ray diffractometer system equipped with kCu_α radiation. Scans were conducted in the range of $2\Theta = 3°–30°$ at a scanning rate of 0.013°/min.

3. Results and discussion

Table 3 summarizes the zeta potential measurements for CL and LP at pH 2 and 7. As expected, both clays exhibited negative zeta potential in acidic and neutral environments [36]. At pH 2, the zeta potential increased significantly, from −37.3 to −12.6 mV for CL and from −25.5 to −2.5 mV for LP. This behavior aligns with earlier studies [36,37]. The variation in zeta potential between CL and LP can be attributed to their mineralogical differences: CL is a montmorillonite-type clay, while LP is hectorite-type. These structural differences influence their chemical composition and the nature of isomorphic substitutions. In acidic pH, the increase in the surface charge can be explained by the replacement of Na^+ ions, which are naturally present in the clay's interlayer space, with H^+ ions. Due to their smaller ionic radius, H^+ ions can be more densely packed within the interlayer region and adsorbed more effectively onto negatively charged sites. This ion exchange leads to a more efficient neutralization of surface charges and a consequent reduction in the overall negative zeta potential [38].

Fig. 2 presents the INH adsorption isotherms of CL and LP at pH 2 and 7, measured at room temperature. The adsorbed INH per gram of clay (n_{ab}, mg/g) is plotted against the equilibrium concentration (C_e, mg/L). Error bars under ±4 % indicate minimal variance. Adsorption capacity for both clays increased under acidic conditions, consistent with enhanced acid-base interactions [3–5,39]. CL adsorption rose from 15 to 115 mg/g, and LP, from 25 to 50 mg/g.

At pH 2, CL exhibited an H2-type curve and LP an L2-type curve, per Giles classification [34,35]. L2 curves signify reduced adsorption with increasing surface saturation, while H2 curves reflect strong adsorbate-adsorbent interactions, as observed for CL at $C_e < 685$ mg/L. Once monolayer capacity was reached, adsorption ceased due to electrostatic repulsion from the protonated INH layer [34,35]. The higher adsorption capacity of CL (115 mg/g) compared to LP (50 mg/g) correlates with zeta potential results, where more negative surface charges reduced electrostatic repulsion [39].

At pH 7, CL exhibited an L3-type isotherm, while LP showed an S3-type curve. L3 isotherms are associated with stable adsorption of individual molecules or small clusters, whereas S3 isotherms indicate a predominance of cluster adsorption [35]. This could explain LP's higher adsorption at pH 7. Initially, the drug fills a monolayer on the clay surface until saturation is achieved. Further addition of the drug forms additional multilayers, consistent with the findings of other works [17,19]. The shape of the adsorption curves varied depending on both the clay type and the pH of the environment (Fig. 2). Indeed, pH influences the protonation state of the drug and the surface charge of the clay, thereby affecting their interaction. INH protonation appears to enhance drug–clay affinity, as reflected in the increased adsorption capacity observed at pH 2 and 7.

The adsorption results were analyzed by fitting them into two different models: the Langmuir and the Freundlich models. The fitted parameters for these models are presented in Table 4. The experimental

Table 3
Zeta potential of CL and LP at pH 2 and pH 7.

Sample	pH 7		pH 2	
	Average (mV)	Dev.	Average (mV)	Dev.
CL	−37.3	1.8	−12.6	0.1
LP	−25.5	4.1	−2.5	0.7

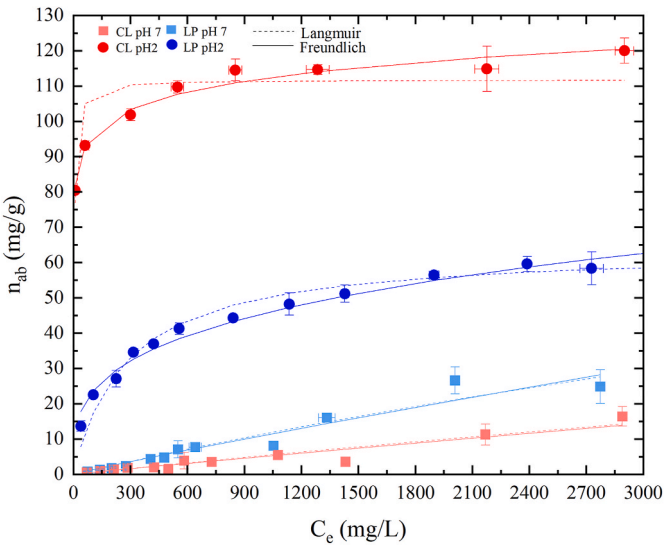

Fig. 2. INH adsorption **isotherms** for CL and LP at pH 2 and pH 7. The adsorption data of LP and CL were discriminated by the colors blue and red, respectively, while square and circle represent the hybrids made at pH 7 and 2, respectively. (For interpretation of the references to color in this figure legend, the reader is referred to the Web version of this article.)

data fitted better into the Freundlich model, indicating that adsorption occurred on a heterogeneous surface, consistent with the clay's structure.

To simulate oral drug release, the INH *in vitro* release profile from CL and LP was evaluated in three media with varying pH: gastric buffer (pH 2) and intestinal buffers (pH 6.8 and 7.4), as shown in Fig. 3 (a). Only samples prepared at pH 2 were used due to their higher adsorption capacity compared to those prepared at pH 7. The cumulative release profiles are expressed as percentages. Consistently small error bars for all samples indicate high precision and reliability. CL/INH exhibited steadily lower cumulative release than LP-INH for all investigated pH levels, particularly at pH 2, where CL showed greater INH affinity. Similar results were observed by other researchers, using montmorillonite as a carrier for INH and other drugs [19,40,41]. The cumulative release of INH increased with pH, reflecting weaker clay-drug interactions. CL released 40 % of INH adsorbed, while LP released 55 %, with neither hybrid achieving full release; the percentages refer to the values of INH adsorbed. The stronger adsorption of INH when using CL likely explains its lower release compared to LP.

To eliminate carryover effects between pH conditions, the release test was performed by exposing the samples separately to pH 2.0 and pH 7.4 for 5 h each. Fig. 3 (b) and (c) show, respectively, the release of INH by LP/INH and CL/INH during 5 h at pH 2 and 7.4. In this study, we managed to remove the influence caused by the previous environment on the release. As can be seen, for both clays, the release at pH 2 followed the tendency observed in the oral release curve, Fig. 3 (a). At the beginning of the release, the INH reached a plateau, and no further release was observed. This result corroborates the adsorption at pH 2. Drug protonation influenced the interaction between the cationic drug and the clay's negative surface charge. As was observed, the lower the clay surface charge, as in CL, the lower the drug release in acidic pH. Indeed, for CL which presented a surface charge of −12.6 mV the release was less than 10 % while for Laponite, which presented a surface charge of −2.5 mV, the release was 25 %. At pH 7.4, for both clays, as expected, the release of the drug increased due to the neutralization of isoniazid and reduced electrostatic interactions. Although few studies have reported on pH-responsive release for comparable systems, the available data suggest our formulation exhibits improved release behavior. For example, Murath et al. (2023) [25] reported pH-dependent release of valsartan and atorvastatin from LDH, with limited release at acidic pH and a slight increase after 5–6 min. Zauska et al. (2022) [26] observed that the acidic form of naproxen had strong interactions with negatively charged surfaces, limiting its release across pH levels. In the case of isoniazid, zeolites released the drug entirely within 10 min with no further increase [5]. In contrast, the clay-based systems investigated here demonstrated a more sustained and controlled release profile, suggesting potential for enhanced therapeutic performance.

Table 5 summarizes the cumulative amount of INH released per gram of clay over time for both hybrids studied in the present work. At the end of the release test, CL released approximately 43 mg/g, while LP released 31 mg/g. Within the first 120 min, at pH 2, LP released approximately 15 mg/g of INH, accounting for nearly 50 % of the total drug release. In contrast, during the same period, the release of CL-INH was less than 20 % of the total amount released, demonstrating a more prolonged release profile. While other carriers such as nanoparticles of silica [4] and palygorskite [3], have shown controlled release behavior, they achieved lower cumulative amount of drug compared to our system. Zeolite carriers exhibited pH- responsive behavior; however, the drug was almost completely released within 10 min, with no further increase observed thereafter [5]. For LDHs, only minimal pH-dependent differences were reported, likely due to testing at pH 4.8, where the protonation effect is less pronounced [13]. Collectively, these comparisons underscore the relevance of our findings: the clay-based systems studied here combine sustained release with higher cumulative drug delivery, offering a potentially more effective platform for oral drug administration.

The release data were fitted to 3 models: zero-order, Korsmeyer-Peppas, and Higuchi. The fitted parameters are provided in Table 6. For CL/INH, at pH 2, none of these models fit the data adequately ($R^2 <$ 0.670). For LP/INH, the Higuchi model provided the best fit ($R^2 =$ 0.984). The release for CL/INH at pH 6.8 was best described by the zero-order model ($R^2 = 0.999$). At pH 7.4, the release data for both hybrids fit the Higuchi model best, indicating that the driving force for release was diffusion, R2 > 0.990. Release behavior was pH-dependent for both clays, though CL was more sensitive to pH changes. At pH 2, CL released only 8 % of INH within the first 2 h, compared to 25 % for LP. This suggests that CL offers enhanced protection for INH in acidic environments, releasing more in response to pH changes. At pH 2, the release profile of CL-INH plateaued within 30 min, with no model providing a strong fit. At pH 6.8, CL-INH followed a Zero-order model, indicating a

Table 4
Both models fitted the adsorption parameters of INH by CL and LP at pH 2 and pH 7.

Clay			CL		LP	
pH			2	7	2	7
Model	Langmuir	K_L (L/mg)	0.2561	$4.0\ 10^{-5}$	0.0036	0.0001
		Q_m (mg/g)	111.7226	133.9961	64.0037	136.8915
		R_L	0.0338	0.9945	0.8147	0.9877
		R^2	**0.7420**	**0.9138**	**0.9674**	**0.9375**
	Freundlich	K_F	70.4641	0.0070	6.1457	0.0186
		N_F	14.8634	1.0500	3.4473	1.0822
		R^2	**0.9747**	**0.9192**	**0.9807**	**0.9312**

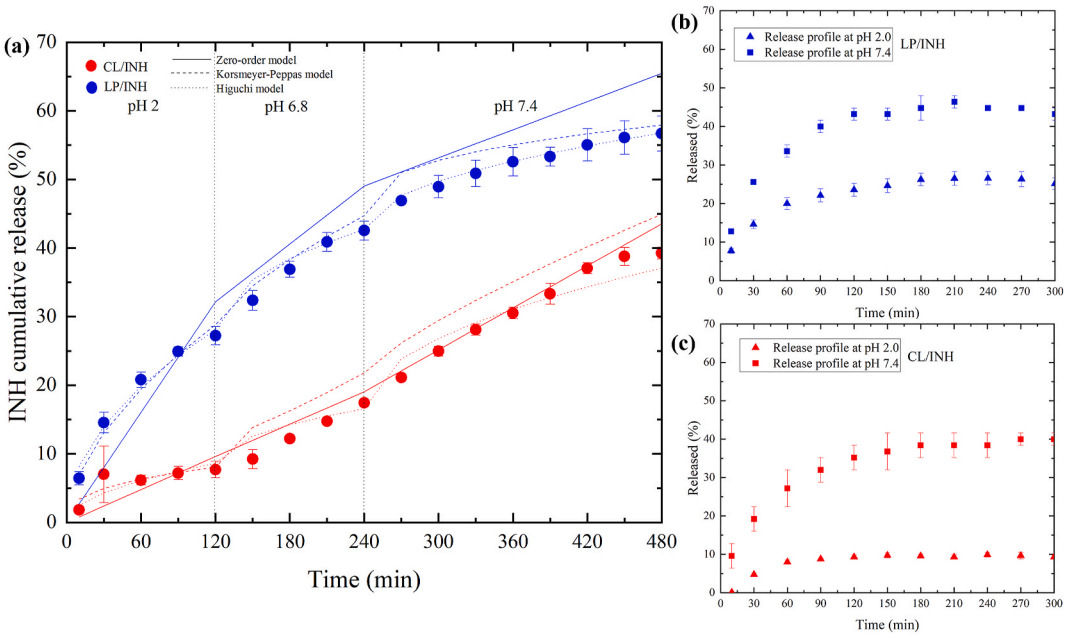

Fig. 3. INH release profiles from CL-INH (red) and LP-INH (blue) hybrids. (a) The release test simulated the oral gastrointestinal pathway: the medium was set to pH 2.0 for 0–120 min, pH 6.8 for 120–240 min, and pH 7.4 for 240–480 min. (b) and (c) show the release profiles at a single pH medium for 300 min, using LP and CL, respectively. Squares represent release at pH 7.4, while triangles indicate release at pH 2.0. (For interpretation of the references to color in this figure legend, the reader is referred to the Web version of this article.)

Table 5
The release of INH in mg/g for the two hybrids studied in oral drug release media: <120 min, pH 2, simulating stomach environment; 120 min < t < 240 min, at pH 6.8, simulating first part of small intestine; t > 240 min, at pH 7.4, simulating the second part of small intestine.

Time	pH	CL/INH		LP/INH	
		INH released (mg/g)	S.D.	INH released (mg/g)	S.D.
10	2	2.0	0.0	3.5	0.0
30		7.7	0.3	7.9	0.1
60		6.8	0.0	11.2	0.1
90		7.9	0.1	13.5	0.1
120		8.5	0.1	14.7	0.2
150	6.8	10.2	0.1	17.5	0.3
180		13.5	0.1	19.9	0.2
210		16.3	0.1	22.1	0.3
240		19.2	0.0	23.0	0.3
270	7.4	23.3	0.1	25.3	0.0
300		27.5	0.2	26.4	0.4
330		31.0	0.3	27.5	0.5
360		33.6	0.3	28.4	0.6
390		36.7	0.6	28.8	0.4
420		40.8	0.3	29.7	0.7
450		42.7	0.6	30.3	0.7
480		43.3	0.4	30.6	0.8

constant release rate independent of drug concentration. In contrast, LP-INH release was diffusion-driven, fitting the Higuchi model. These findings highlight the significant role of clay-drug interactions and release conditions in controlling INH release, with CL providing greater stability in acidic environments compared to LP.

Fig. 4 displays the TGA curves for the pristine clays and their respective hybrids. The weight loss of the clays occurred in three major steps: first, due to the loss of surface water molecules; second, from the loss of hydration water, and finally, due to dehydroxylation [17]. The TGA curves for CL/INH and LP/INH exhibited additional degradation steps due to the incorporation of INH.

The mass loss of pristine clays and their respective hybrids is summarized in Table 7. The weight loss during the first stage of clay degradation was similar for each clay and their corresponding hybrid. Most differences emerged in the second stage: CL lost 3.1 % of its mass, and CL/INH lost 7.1 %. Similarly, LP lost 6.2 %, while LP/INH lost 10.4 %. This increase in weight loss can be attributed to the degradation of INH by around 220 °C [18].

Fig. 5 shows the DTG curves for INH, pristine clays, and their respective hybrids. The degradation of INH occurred with two peaks at approximately 237 °C and 305 °C. The curves for the pristine clays exhibited only two peaks, corresponding to the mass loss of surface water, around 100 °C, and dehydroxylation, around 636 °C and 730 °C, for CL and LP, respectively. For CL/INH, the emergence of a peak around 356 °C and the downward shift of dehydroxylation from 639 to 600 °C are likely attributable to the overlapping of the decomposition of INH

Table 6
Release fitting of CL/INH and LP/INH hybrids made at pH 2 and 7.

Release pH	Hybrid	Zero Order		Korsmeyer-Peppas			Higuchi	
		K_o	R^2	k_1	n	R^2	K_o	R^2
pH **2**	CL/INH	0.080	0.557	1.516	0.349	0.706	0.788	**0.670**
	LP/INH	0.268	0.922	1.884	0.570	0.978	2.567	**0.984**
pH **6.8**	CL/INH	0.079	**0.999**	0.032	1.195	0.995	1.324	0.990
	LP/INH	0.141	0.964	0.450	0.744	0.979	0.905	**0.996**
pH **7.4**	CL/INH	0.102	0.978	0.290	0.799	0.987	1.324	**0.990**
	LP/INH	0.069	0.976	1.877	0.356	0.994	0.905	**0.996**

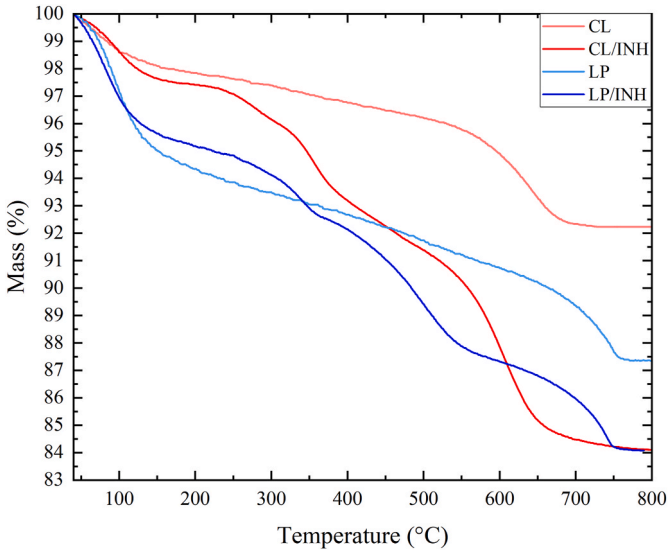

Fig. 4. TGA of pristine clays and their respective hybrids made at pH 2.

and the dehydroxylation process. In the case of LP/INH, two peaks appeared around 346 and 505 °C for the same reason [42]. This phenomenon, the increase of INH degradation, may have occurred due to the thermal protection provided by LP and CL, which enhanced the degradation of INH. Similar results were observed in other studies as well [5]. According to these studies, the peak around 350 °C corresponds to the degradation of weakly adsorbed INH, while the degradation observed at higher temperatures indicates that a portion of INH is strongly bound to the clay particles.

The FTIR spectra of INH, pristine clays, and their respective hybrids are shown in Fig. 6. The CL/INH spectra exhibited more prominent INH bands than the LP/INH spectrum, which can be attributed to the higher amount of INH incorporated by the former. The bands 751, 851, 1324, and 1681 cm^{-1} were common to both hybrids, while CL/INH also presented the bands around 1545, 1496, and 891 cm^{-1}. Additionally, the Si–OH peaks for both clays shifted after INH incorporation: from 995 to 1013 cm^{-1} for LP, and from 999 to 1004 cm^{-1} for CL. Furthermore, the peak at 1681 cm^{-1} that appeared in both hybrid spectra corresponds to a band shift of 1663 cm^{-1} of INH indicating the interaction between the clay and INH [16,17]. The INH bands in both clay/INH spectra indicated an interaction between the drug and the clays. The band around 1663 cm^{-1}, attributed to amide carbonyl vibrations of INH, shifted to 1683 cm^{-1} for both hybrids. This positive shift suggests the formation of H-bonds between the drug and clay. The band shifted around 1000 cm^{-1} in both clays to 1004 for CL and 1013 cm^{-1} for LP, further indicating an interaction between drug and siloxane clay groups (Si–*O*–Si) [4]. The bands around 1545 and 1496 cm^{-1} can be assigned to the ring stretching vibration while the bands around 851 and 751 cm^{-1} may be assigned to the out-of-plane deformation modes of the aromatic ring [5]. Previous studies have reported similar findings, indicating that exo and endo-cyclic nitrogen atoms were involved in the interaction between clay and INH [16,17]. More INH bands appeared in the CL/INH spectrum than in the LP/INH spectrum due to the higher amount of INH incorporated in the CL hybrid.

Fig. 7 displays the XRD patterns for INH, pristine clays, and their respective hybrids. None of the diffractograms for the clay-drug hybrids show the initial peaks of INH, as was observed in other studies [17], which may suggest that the drug did not crystallize on the clay surface. The basal peak of CL shifted from 1.18 nm to 1.28 nm, while the basal peak of LP did not exhibit a change. Similar results were found in other studies [40]. When comparing pristine clays and their hybrids, the 001 reflection ($2\theta \approx 7°$) appears more defined after INH incorporation. The narrowing of this peak suggests enhanced structural organization, possibly due to physicochemical interactions between the clay and the drug. This interaction may promote partial rearrangement of the clay platelets, even in the absence of a significant increase in interlayer spacing, indicating that a portion of the drug might be intercalated between the layers. Additionally, the 001 peak of LP is broader than that of CL, which is consistent with its smaller platelet size and reduced preferred orientation along the z-axis.

XRD showed that the interaction with the drug can increase clay crystallization (Fig. 7), TGA indicated that both clays protected the drug from thermal degradation (Figs. 4 and 5), and FTIR demonstrated the interaction between clay and drug (Fig. 6). TGA confirmed INH adsorption by clays, and DTG curves showed that INH degradation occurred at higher temperatures, after adsorption of the INH by the clays, indicating protection provided by the clay's particles. Additionally, for LP, the peak degradation temperatures of the drug on the DTG shifted from 287 °C to 332–346 °C and 505 °C, respectively. For CL/INH,

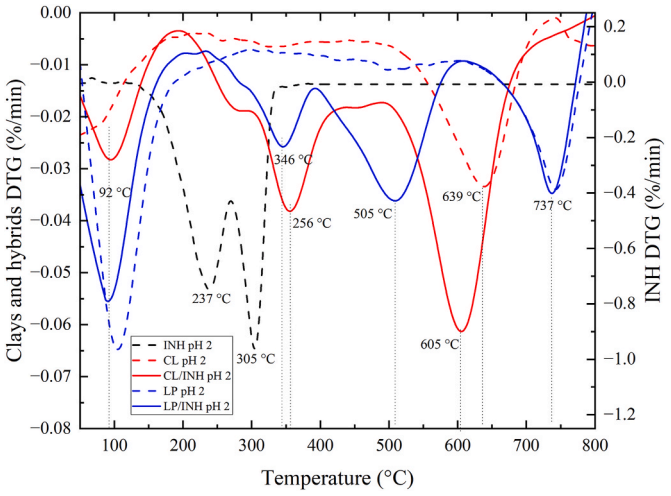

Fig. 5. DTG of LP, LP/INH, CL, and CL/INH prepared at pH 2, and DTG of INH after being treated at pH 2.

Table 7
Weight loss of CL, LP, and their hybrids.

Stage	CL		CL/INH		LP		LP/INH	
	Temperature range (°C)	Weight loss (%)	Temperature range (°C)	Weight loss (%)	Temperature range (°C)	Weight loss (%)	Temperature range (°C)	Weight loss (%)
1st stage	40–110	1.5	40–146	2.3	40–133	4.5	40–121	3.8
2nd stage	120–579	3.1	146–237	0.5	133–705	6.2	121–309	2.2
			237–340	2.0			309–356	1.3
			340–554	5.1			356–548	4.8
							548–706	2.1
3rd stage	579–684	3.0	554–657	5.2	705–756	1.9	706–751	1.6

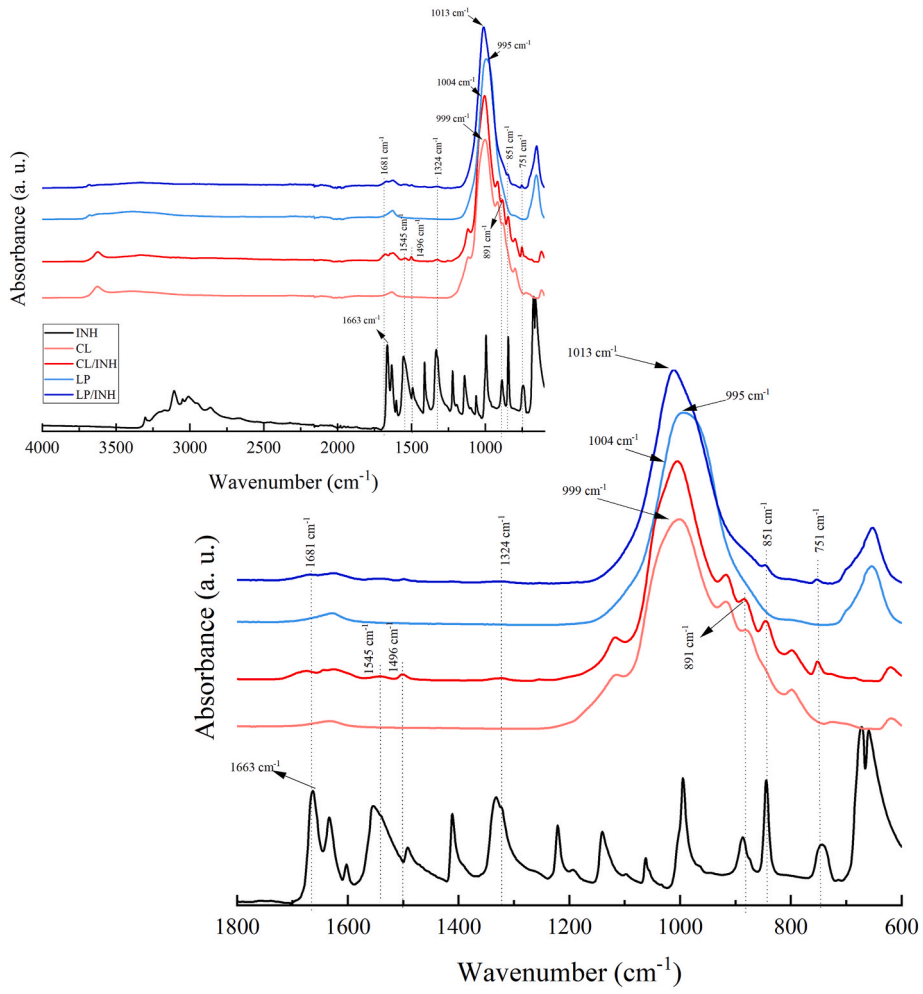

Fig. 6. FTIR spectra of INH, CL, LP, CL/INH, and LP/INH at pH 2.

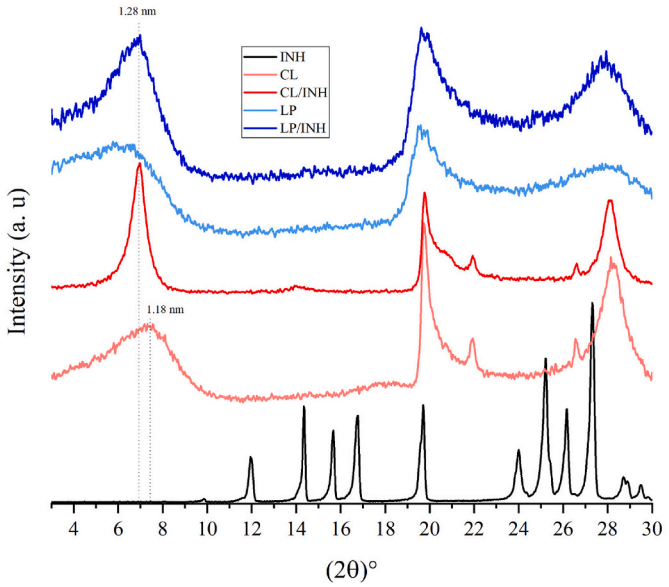

Fig. 7. XRD patterns of CL and LP clays and hybrids made at pH 2.

the INH degradation occurred at 356 °C and 605 °C. It was also noted that the dehydroxylation peak of LP around 737 °C remained unchanged after INH incorporation, while the CL peak decreased by 30 °C. This occurred because of the overlapping of drug degradation and clay dehydroxylation. The fact that CL increased the degradation temperature more than LP further supports the adsorption and release results indicating that CL had stronger interactions with INH than LP.

4. Conclusion

Two types of clays, cloisite (CL) and laponite (LP), were investigated for isoniazid (INH) adsorption and release efficiency, with CL being found to be superior to LP. INH adsorption by CL at pH 2 resulted in a significant adsorption ratio of mg/g compared to pH 7 due to an acid-base attraction. Minimal release by this clay was observed at a pH of 2, corresponding to the stomach conditions (around 8 % of the drug incorporated, 9 mg/g), and this was prolonged for up to 5 h. In the case of LP, around 25 % of the drug was released at the same pH. This shows that the pH had a higher effect in CL, probably due to its lower surface charge, increasing the interaction with INH. For the same reason, the CL/INH hybrid showed an excellent adsorption ratio of 115 mg/g, and superior release at pH 6.8 and 7.4, corresponding to the conditions of the small intestine following the zero-order model. The importance of the interaction between the carrier and the drug was demonstrated by comparing clays with the same physical structure (pillared lamellas), but different chemical compositions. The protonation effect was utilized to maximize the drug intake into CL and LP at a pH equal to 2 while minimizing drug release in the stomach at the same pH.

Despite the promising results presented here, several limitations should be acknowledged. For instance, the potential for clay aggregation

under physiological conditions – and its effect on drug release and bioavailability - remains to be investigated. Additionally, although the *in vitro* release studies are encouraging, further biological validation is required, including cytotoxicity assays, biocompatibility assessments, and *in vivo* evaluations to confirm the safety and efficacy of these systems. Future studies could also incorporate computational modeling to gain deeper insight into the interaction mechanisms between INH and clay surfaces at the molecular level. Such understanding would support the rational design and optimization of next-generation clay-based drug delivery platforms.

CRediT authorship contribution statement

Jessica de Carvalho Arjona: Writing – review & editing, Writing – original draft, Visualization, Validation, Software, Methodology, Investigation, Formal analysis, Data curation, Conceptualization. **Mazen Samara:** Writing – review & editing, Visualization, Validation. **Carina Ulsen:** Writing – review & editing, Validation, Software, Methodology, Data curation. **Francisco Rolando Valenzuela Diaz:** Writing – review & editing, Visualization, Validation, Supervision, Project administration, Methodology, Investigation, Funding acquisition, Data curation, Conceptualization. **Nicole Raymonde Demarquette:** Writing – review & editing, Visualization, Validation, Supervision, Resources, Project administration, Methodology, Funding acquisition, Conceptualization.

Funding sources

Funding: This work was supported by the CNPq (*Conselho Nacional de Desenvolvimento Científico e Tecnológico*), grant number 141859/2020–2; CAPES (*Coordenação de Aperfeiçoamento de Pessoal de Nível Superior*), grant number 88887.694663/2022–00; FAPESP (*Fundação de Amparo à Pesquisa do Estado de São Paulo*), grant number 2019/01231–2 and 2022/00662–2; and NSERC (Natural Sciences and Engineering Research Council of Canada), grant number ALLRP 573019–22 as well Canadian Research Chair Tier 1.

During the preparation of this work, the authors used ChatGPT to refine and improve the clarity and grammar of certain sentences. However, it was solely employed for language enhancement, without contributing to the generation of any scientific content or ideas. After using this tool/service, the authors reviewed and edited the content as needed and took full responsibility for the publication's content.

Declaration of competing interest

The authors declare that they have no known competing financial interests or personal relationships that could have appeared to influence the work reported in this paper.

Acknowledgments

The authors also would like to acknowledge and express gratitude for the infra-structural assistance provided by LIPEC-PolymerETS (*Laboratoire d'ingénierie des polymères et composites* at ÉTS) and STEPPE (*Station Expérimentale des Procédés Pilotes en Environnement* at ÉTS). As well Dr. Maria das Graças Silva-Valenzuela for her expertise and assistance throughout this study, and the undergraduate student Ms. Colyne Jacques for her assistance in conducting some of the adsorption and release tests.

Data availability

Data will be made available on request.

References

[1] R. C, James C. Johnston, D. Menzies, Chapter 5: treatment of tuberculosis disease, Canadian J.Respiratory, Critical Care, Sleep Med. 6 (2022) 66–76, https://doi.org/10.1080/24745332.2022.2036504.

[2] E. Carazo, G. Sandri, P. Cerezo, C. Lanni, F. Ferrari, C. Bonferoni, C. Viseras, C. Aguzzi, Halloysite nanotubes as tools to improve the actual challenge of fixed doses combinations in tuberculosis treatment, J. Biomed. Mater. Res. 107 (2019) 1513–1521, https://doi.org/10.1002/jbm.a.36664.

[3] E. Damasceno Junior, J.M.F. de Almeida, I. do N. Silva, M.L. Moreira de Assis, L. M. dos Santos, E.F. Dias, V.E. Bezerra Aragão, L.M. Veríssimo, N.S. Fernandes, D. R. da Silva, E.D. Junior, J. Mayara, F. De Almeida, N. Silva, M. Lizandra, M. De Assis, L. Maciel, E.F. Dias, V. Eduardo, B. Aragão, L.M. Veríssimo, N.S. Fernandes, D. Ribeiro, pH-responsive release system of isoniazid using palygorskite as a nanocarrier, J. Drug Deliv. Sci. Technol. 55 (2019) 101399, https://doi.org/10.1016/j.jddst.2019.101399.

[4] J.M.F. de Almeida, E. Damasceno Júnior, L.M. Verrísimo, N.S. Fernandes, pH-Dependent release system of isoniazid carried on nanoparticles of silica obtained from expanded perlite, Appl. Surf. Sci. 489 (2019) 297–312, https://doi.org/10.1016/j.apsusc.2019.05.317.

[5] I.M.S. Souza, A. Borrego-Sánchez, C.I. Sainz-Díaz, C. Viseras, S.B.C. Pergher, Study of Faujasite zeolite as a modified delivery carrier for isoniazid, Mater. Sci. Eng. C 118 (2021) 12, https://doi.org/10.1016/j.msec.2020.111365.

[6] M. Gajendiran, H. Jo, K. Kim, S. Balasubramanian, In vitro controlled release of tuberculosis drugs by amphiphilic branched copolymer nanoparticles, J. Ind. Eng. Chem. 77 (2019) 181–188, https://doi.org/10.1016/j.jiec.2019.04.033.

[7] N. Devi, T.K. Maji, Genipin crosslinked chitosan'k-carrageenan polyelectrolyte nanocapsules for the controlled delivery of isoniazid, Int. J.Polymeric Materi. Polymeric Biomater. 59 (2010) 828–841, https://doi.org/10.1080/00914037.2010.484792.

[8] R.M. Lucinda-Silva, R.C. Evangelista, Microspheres of alginate-chitosan containing isoniazid, J. Microencapsul. 20 (2003) 145–152, https://doi.org/10.1080/02652040210162621.

[9] S.C. Angadi, L.S. Manjeshwar, T.M. Aminabhavi, Interpenetrating polymer network blend microspheres of chitosan and hydroxyethyl cellulose for controlled release of isoniazid, Int. J. Biol. Macromol. 47 (2010) 171–179, https://doi.org/10.1016/j.ijbiomac.2010.05.003.

[10] P.M. Oliveira, B.N. Matos, P.A.T. Pereira, T. Gratieri, L.H. Faccioli, M.S.S. Cunha-Filho, G.M. Gelfuso, Microparticles prepared with 50–190 kDa chitosan as promising non-toxic carriers for pulmonary delivery of isoniazid, Carbohydr. Polym. 174 (2017) 421–431, https://doi.org/10.1016/j.carbpol.2017.06.090.

[11] N. Genina, J.P. Boetker, S. Colombo, N. Harmankaya, J. Rantanen, A. Bohr, Anti-tuberculosis drug combination for controlled oral delivery using 3D printed compartmental dosage forms: from drug product design to in vivo testing, J. Contr. Release 268 (2017) 40–48, https://doi.org/10.1016/j.jconrel.2017.10.003.

[12] I.M.S. Souza, C.I. Sainz-Díaz, C. Viseras, S.B.C. Pergher, Adsorption capacity evaluation of zeolites as carrier of isoniazid, Microporous Mesoporous Mater. 292 (2020), https://doi.org/10.1016/j.micromeso.2019.109733.

[13] B. Saifullah, M.E. El Zowalaty, P. Arulselvan, S. Fakurazi, T.J. Webster, B. M. Geilich, M.Z. Hussein, Synthesis, characterization, and efficacy of antituberculosis isoniazid zinc aluminum-layered double hydroxide based nanocomposites, Int. J. Nanomed. 11 (2016) 3225–3237, https://doi.org/10.2147/IJN.S102406.

[14] E. Carazo, A. Borrego-Sánchez, F. García-Villén, R. Sánchez-Espejo, C. Viseras, P. Cerezo, C. Aguzzi, Adsorption and characterization of palygorskite-isoniazid nanohybrids, Appl. Clay Sci. 160 (2018) 180–185, https://doi.org/10.1016/j.clay.2017.12.027.

[15] S. Akyuz, T. Akyuz, E. Akalin, Adsorption of isoniazid onto sepiolite-palygorskite group of clays: an IR study, Spectrochim. Acta Mol. Biomol. Spectrosc. 75 (2010) 1304–1307, https://doi.org/10.1016/j.saa.2009.12.069.

[16] S. Akyuz, T. Akyuz, FT-IR and FT-Raman spectroscopic studies of adsorption of isoniazid by montmorillonite and saponite, Vib. Spectrosc. 48 (2008) 229–232, https://doi.org/10.1016/j.vibspec.2008.02.019.

[17] E. Carazo, A. Borrego-Sánchez, R. Sánchez-Espejo, F. García-Villén, P. Cerezo, C. Aguzzi, C. Viseras, Kinetic and thermodynamic assessment on isoniazid/montmorillonite adsorption, Appl. Clay Sci. 165 (2018) 82–90, https://doi.org/10.1016/j.clay.2018.08.009.

[18] J. de Carvalho Arjona, C. Ulsen, F.R. Valenzuela-Diaz, N.R. Demarquette, Influence of smectite clays' pores volume on isoniazid adsorption and release, Appl. Clay Sci. 252 (2024), https://doi.org/10.1016/j.clay.2024.107341.

[19] J. de Carvalho Arjona, C. Ulsen, D. Tada, F.R. Valenzuela Diaz, N.R. Demarquette, The influence of adsorption incorporation mechanism on the release of isoniazid by montmorillonite, J. Drug Deliv. Sci. Technol. (2025) 106809, https://doi.org/10.1016/j.jddst.2025.106809.

[20] E. Carazo, A. Borrego-Sánchez, F. García-Villén, R. Sánchez-Espejo, C. Aguzzi, C. Viseras, C.I. Sainz-Díaz, P. Cerezo, Assessment of halloysite nanotubes as vehicles of isoniazid, Colloids Surf. B Biointerfaces 160 (2017) 337–344, https://doi.org/10.1016/j.colsurfb.2017.09.036.

[21] G. Chen, Y. Wu, D. Yu, R. Li, Isoniazid-loaded chitosan/carbon nanotubes microspheres promote secondary wound healing of bone tuberculosis, J. Biomater. Appl. 33 (2018) 989–996, https://doi.org/10.1177/0885328218814988.

[22] N. Banik, A. Ramteke, T.K. Maji, Carboxymethyl chitosan-montmorillonite nanoparticles for controlled delivery of isoniazid: evaluation of the effect of the glutaraldehyde and montmorillonite, Polym. Adv. Technol. 25 (2014) 1580–1589, https://doi.org/10.1002/pat.3406.

[23] N. Banik, A. Hussain, A. Ramteke, H.K. Sharma, T.K. Maji, Preparation and evaluation of the effect of particle size on the properties of chitosan-montmorillonite nanoparticles loaded with isoniazid, RSC Adv. 2 (2012) 10519–10528, https://doi.org/10.1039/c2ra20702h.
[24] C. Saikia, A. Hussain, A. Ramteke, H.K. Sharma, T.K. Maji, Carboxymethyl starch-chitosan-coated iron oxide magnetic nanoparticles for controlled delivery of isoniazid, J. Microencapsul. 32 (2015) 29–39, https://doi.org/10.3109/02652048.2014.940015.
[25] S. Muráth, N. Dvorníková, D. Moreno-Rodríguez, R. Novotný, M. Pospíšil, M. Urbanová, J. Brus, F. Kovanda, Intercalation of atorvastatin and valsartan into Mg[sbnd]Al layered double hydroxide host using a restacking procedure, Appl. Clay Sci. 231 (2023), https://doi.org/10.1016/j.clay.2022.106717.
[26] Ľ. Zauška, E. Beňová, M. Urbanová, J. Brus, V. Zeleňák, V. Hornebecq, M. Almáši, Adsorption and release properties of drug delivery system Naproxen-SBA-15: effect of surface polarity, Sodium/Acid drug form and pH, J. Funct. Biomater. 13 (2022), https://doi.org/10.3390/jfb13040275.
[27] G. Kiaee, N. Dimitrakakis, S. Sharifzadeh, H.J. Kim, R.K. Avery, K.M. Moghaddam, R. Haghniaz, E.P. Yalcintas, N.R. de Barros, S. Karamikamkar, A. Libanori, A. Khademhosseini, P. Khoshakhlagh, Laponite-Based nanomaterials for drug delivery, Adv. Healthcare Mater. 11 (2022) 1–21, https://doi.org/10.1002/adhm.202102054.
[28] A.S. Oliveira, A.C.S. Alcântara, S.B.C. Pergher, Bionanocomposite systems based on montmorillonite and biopolymers for the controlled release of olanzapine, Mater. Sci. Eng. C 75 (2017) 1250–1258, https://doi.org/10.1016/j.msec.2017.03.044.
[29] G. Lagaly, M.F. Gonzalez, A. Weiss, Problems in layer-charge determination of montmorillonites, Clay Miner. 11 (1976) 173–187.
[30] C. Nomicisio, M. Ruggeri, E. Bianchi, B. Vigani, C. Valentino, C. Aguzzi, C. Viseras, S. Rossi, G. Sandri, Natural and synthetic clay minerals in the pharmaceutical and biomedical fields, Pharmaceutics 15 (2023), https://doi.org/10.3390/pharmaceutics15051368.
[31] M.A. Djebbi, S. Boubakri, Z. Bouaziz, M.S. Elayachi, P. Namour, N. Jaffrezic-Renault, A. Ben Haj Amara, Extended-release of chlorpromazine intercalated into montmorillonite clays, Microporous Mesoporous Mater. 267 (2018) 43–52, https://doi.org/10.1016/j.micromeso.2018.03.017.
[32] S.A. Martín, I. Pérez, A. Rivera, Hosting of the antibiotic Vancomycin by bentonite: characterization and slow release study, Appl. Clay Sci. 202 (2021), https://doi.org/10.1016/j.clay.2020.105965.
[33] C.V.L. Natarelli, P.I.C. Claro, K.W.E. Miranda, G.M.D. Ferreira, J.E. de Oliveira, J. M. Marconcini, 2,4-Dichlorophenoxyacetic acid adsorption on montmorillonite organoclay for controlled release applications, SN Appl. Sci. 1 (2019), https://doi.org/10.1007/s42452-019-1235-4.
[34] C.H. Giles, D. Smith, A general treatment and classification of the solute adsorption isotherm, Journal of Co 47 (1974) 755–765, https://doi.org/10.1007/s41193-016-0111-5.
[35] C.H. Giles, T.H. MacEwan, S.N. Nakhwa, D. Smith, Studies in adsorption. Part XI. A system of classification of solution adsorption isotherms, and its use in diagnosis of adsorption mechanisms and in measurement of specific surface areas of solids, J. Chem. Soc. (1960) 3973–3993, https://doi.org/10.1039/jr9600003973.
[36] I. Ghorbel-Abid, C. Vagner, R. Denoyel, M. Trabelsi-Ayadi, Effect of cadmium and chromium adsorption on the zeta potential of clays, Desalination Water Treat. 57 (2016) 17128–17138, https://doi.org/10.1080/19443994.2015.1134350.
[37] M. Chorom, P. Rengasamy, Dispersion and zeta potential of pure clays as related to net particle charge under varying pH, electrolyte concentration and cation type, Eur. J. Soil Sci. 46 (1995) 657–665.
[38] A. Delgado, F. Gonzalez-Caballero, J.M. Bruque, On the Zeta Potential and Surface Charge Density of Montmorillonite in Aqueous Electrolyte Solutions, 1986.
[39] E. Çalışkan Salihi, Z. Gündüz, A.S. Başţuğ, E.Ç. Salihi, Z. Gündüz, A.S. Başţuğ, Fast retention of isoniazid on organobentonite prepared using green chemistry approach: contribution of the π interactions, Separ. Sci. Technol. 54 (2019) 2695–2705, https://doi.org/10.1080/01496395.2018.1543324.
[40] I. Calabrese, G. Cavallaro, C. Scialabba, M. Licciardi, M. Merli, L. Sciascia, M. L. Turco Liveri, Montmorillonite nanodevices for the Colon metronidazole delivery, Int. J. Pharm. 457 (2013) 224–236, https://doi.org/10.1016/j.ijpharm.2013.09.017.
[41] L. Sciascia, I. Calabrese, G. Cavallaro, M. Merli, C. Scialabba, M.L.T. Liveri, Modified montmorillonite as drug delivery agent for enhancing antibiotic therapy, Minerals 11 (2021), https://doi.org/10.3390/min11121315.
[42] G.V. Joshi, B.D. Kevadiya, H.C. Bajaj, Design and evaluation of controlled drug delivery system of buspirone using inorganic layered clay mineral, Microporous Mesoporous Mater. 132 (2010) 526–530, https://doi.org/10.1016/j.micromeso.2010.04.003.